

AN ADAPTIVE MESH REFINEMENT ALGORITHM FOR THE DISCRETE ORDINATES METHOD

J. Patrick Jessee and Woodrow A. Fiveland

Research and Development Division
Babcock & Wilcox
Alliance, Ohio 44601
patrick.jessee@mcdermott.com

Louis H. Howell, Phillip Colella, and Richard B. Pember

Center for Computational Sciences & Engineering
Lawrence Berkeley National Laboratory
Berkeley, CA 94720

ABSTRACT

The discrete ordinates form of the radiative transport equation (RTE) is spatially discretized and solved using an adaptive mesh refinement (AMR) algorithm. This technique permits the local grid refinement to minimize spatial discretization error of the RTE. An error estimator is applied to define regions for local grid refinement; overlapping refined grids are recursively placed in these regions; and the RTE is then solved over the entire domain. The procedure continues until the spatial discretization error has been reduced to a sufficient level. The following aspects of the algorithm are discussed: error estimation, grid generation, communication between refined levels, and solution sequencing. This initial formulation employs the step scheme, and is valid for absorbing and isotropically scattering media in two-dimensional enclosures. The utility of the algorithm is tested by comparing the convergence characteristics and accuracy to those of the standard single-grid algorithm for several benchmark cases. The AMR algorithm provides a reduction in memory requirements and maintains the convergence characteristics of the standard single-grid algorithm; however, the cases illustrate that efficiency gains of the AMR algorithm will not be fully realized until three-dimensional geometries are considered.

NOMENCLATURE

C	set of ordered grids
E	error, %
G	incident energy, W/m^2
I	intensity, $W/m^2\text{-sr}$
L	transport operator
M	total number of discrete ordinates directions
N_{cell}	number of control volumes in computation mesh
N^l	number of rectangular grids in level l
n	surface normal
P	projection operator
r	position vector, m
R	residual
s	path length, m

S	source term, $W/m^3\text{-sr}$
S_n	order of discrete ordinates approximation
t	time, s
V	volume, m^3
w_k	direction weights
x,y,z	coordinate directions, m
β	extinction coefficient ($= \kappa + \sigma$), m^{-1}
Γ	domain boundary
ϵ	emissivity
θ	error tolerance
κ	absorption coefficient, m^{-1}
Λ	spatial domain
$\partial\Lambda$	domain boundary
μ,ξ,η	direction cosines
ρ	reflectivity ($= 1-\epsilon$)
σ	scattering coefficient, m^{-1}
Ω	direction with direction cosines (μ,ξ,η)

Superscripts

e	external
i	internal
l	level
l_{max}	finest refinement level
n	iteration
o	reference

Subscripts

m	direction
b	blackbody
i, j	nodal indices
k	generic index
n	n^{th} S_n approximation

Miscellaneous

'	incoming direction
bold	vectorial quantity
-	exact value, average value
$\langle \cdot \rangle$	spatial averaging operator

INTRODUCTION

Most practical combustion applications exhibit a variety of length scales with some regions of the spatial domain containing much higher gradients than others. In addition, some applications involve moving fronts where the location and shape of the reaction zone change over time. To accurately predict the physical processes using a numerical model, the density of nodes or control volumes must be very high in the regions with steep gradients and may need to be spatially adapted over time to conform to the state of the fluid. Much progress has been made in the computational fluid dynamics community in developing spatial and temporal adaptation algorithms to accurately predict the fluid dynamic processes with such disparate length and time scales (Bell et al., 1994; Fuchs, 1986; and Kallinderis, 1992).

In addition to convective and diffusive transport associated with fluid dynamics, radiative heat transfer often plays a large role in governing combustion dynamics. Radiative heat transfer is the dominant mode of heat transfer in many combustion applications and may significantly affect gas and wall temperatures. Because reaction rates and density distributions are closely linked to the local gas temperatures, radiative heat transfer may be very influential in combustion dynamics. Unfortunately, most deterministic methods for predicting radiative heat transfer have only been formulated for fixed computational grids which cannot support the locally refined grid structure necessary for resolving steep solution gradients and adapting to changing conditions. In this respect, the development of adaptive radiation techniques has largely lagged work in the computational fluid dynamics community.

The discrete ordinates (DO) method has been widely applied to multi-dimensional radiative heat transfer with participating media. The method requires a single formulation to invoke higher order approximations, integrates easily into control volume transport codes, guarantees conservation of radiant energy, and is applicable to non-gray (Fiveland and Jamaluddin, 1991) and anisotropically scattering media (Fiveland, 1988). Based on these characteristics, the DO method has been selected for implementation into a adaptive mesh refinement environment.

The primary objective of this paper is to lay the foundation for applying the DO method in the context of spatial/temporal adaptation. The methodology parallels the work of Bell et al. (1994) for the compressible Navier-Stokes equations, and is intended to complement the work being done at the Center for Computational Sciences & Engineering at Lawrence Berkeley National Laboratory. Methods outlined herein build on the existing software base for adaptive grid techniques, and are compatible with the approach taken in the fluid dynamic development.

The remainder of the paper is broken into four sections. Section 2 presents the governing equations -- the radiative transport equation and DO approximation. Section 3 details the adaptive mesh refinement (AMR) algorithm, while results from the algorithm are presented and discussed in Section 4. Finally, Section 5 summarizes the work and states conclusions based on the considered cases.

2.0 GOVERNING EQUATIONS

2.1 Radiative Transport Equation

This paper considers an emitting-absorbing and isotropically scattering gray medium, although the discrete ordinates method is not restricted to these conditions. For this medium, the radiative transport equation (RTE) is:

$$(\Omega \cdot \nabla) I(r, \Omega) = - (\kappa + \sigma) I(r, \Omega) + \frac{\sigma}{4\pi} \int_{4\pi} I(r, \Omega') d\Omega' + \kappa I_b(r) \tag{1}$$

where $I(r, \Omega)$ is the radiation intensity; $I_b(r)$ is the intensity of blackbody radiation at the temperature of the medium; and κ and σ are the gray absorption and scattering coefficients of the medium, respectively. This integro-differential equation, which governs the radiative heat transfer in a general spatial domain Λ , has both spatial and angular dependence.

For gray surfaces which reflect diffusely, the radiative boundary condition for Equation (1) is given by:

$$I(r, \Omega) = \epsilon I_b(r) + \frac{\rho}{\pi} \int_{\mathbf{n} \cdot \Omega' < 0} |\mathbf{n} \cdot \Omega'| I(r, \Omega') d\Omega' \tag{2}$$

where r belongs to the domain boundary Γ and Equation (2) applies for $\Omega \cdot \mathbf{n} > 0$. $I(r, \Omega)$ is the intensity leaving a surface at a boundary condition location, ϵ is the surface emissivity, ρ is the surface reflectivity, and \mathbf{n} is the unit normal vector at the boundary location.

2.2 Discrete Ordinates Method

The discrete ordinates method is a general method for solving the neutron or radiative transport equations. Only an overview will be given here since the method has been detailed elsewhere (Lewis and Miller, 1984; Modest, 1993). The numerical solution of the RTE requires discretization of both spatial and angular domains. Formally, the discrete ordinates method only pertains to the angular discretization. Spatial and angular discretizations are typically performed independently, with the angular discretization performed first.

In the discrete ordinates method, the governing RTE is replaced by a discrete set of equations for a finite number of directions, Ω_m , and each integral is replaced by a quadrature:

$$(\Omega_m \cdot \nabla) I(r, \Omega_m) = - \beta I(r, \Omega_m) + \frac{\sigma}{4\pi} \sum_{k=1}^M w_k I(r, \Omega_k) + \kappa I_b \tag{3}$$

where w_k are the ordinate weights. This angular approximation transforms the original integro-differential equation into a set of coupled differential equations. Weights and directions are commonly based on the S_n approximation (Fiveland, 1988, 1991). To simplify the presentation of the algorithm, the notation in Equation (3) is simplified as follows:

$$L_m(I_m) = \kappa I_b + S_m \tag{4}$$

where S_m denotes the in-scattering source term, and the operator L_m is defined as

$$L_m = (\Omega_m \cdot \nabla) + \beta \tag{5}$$

After angular discretization has been performed, the DO equations may be discretized spatially using a number of techniques. Of the various techniques, the finite volume method (also known as the control volume method) is most widely used, principally because the method guarantees conservation of radiant energy, is computationally inexpensive, and is intuitively based. To reduce storage requirements, the transport equation for each ordinate direction is usually discretized

and solved independently. In-scattering source terms and reflected boundary conditions are updated through global iteration.

3.0 SOLUTION METHODS

3.1 Adaptive Mesh Refinement (AMR) Algorithm

The present algorithm focuses on solution of the steady-state RTE over a computational domain; the transient term of the RTE may be neglected for most practical problems as it is scaled by the inverse of the speed of light. Eventually, the algorithm is intended for integration into a transient, gas-phase combustion code which is based on the same grid structure and discretization methodology. Upon integration, the steady RTE calculations will be performed every time-step, and coupling to the advective-diffusive energy transport equation will be considered. For coupled, transient calculations, regridding occurs at a prescribed time interval to track moving fronts of the developing flow field. The present algorithm for pure radiation calculations, which has stationary forcing functions (i.e. emissive power), differs from the transient algorithm in that grid adaption occurs after a complete solution to the RTE is obtained.

The development of the AMR algorithm for radiation transport follows the course taken by Bell et al. (1994) for fluid dynamics. The governing equations are integrated (solved) over an hierarchial grid

structure in which the grids have differing levels of refinement. The grid structure is based on a estimation of solution error; highly refined grids are placed in regions of the domain with relatively high spatial discretization error. The algorithm proceeds as follows: the discrete RTE is solved to some level of convergence on a given grid structure, an estimation of error is made, a new grid structure is generated, and the RTE is solved again. The process continues until the error has been reduced to a sufficient level.

Because the fluid dynamic and radiation modules are eventually intended to be closely coupled to perform combustion dynamics calculations, the grid structures for the two physics modules will most likely be the same. Generally, the distribution of local truncation error for the two modules, on which grid refinement is based, will not be the same due to the differing physical processes and to different variations in fluid dynamic and optical properties. Consequently, for coupled calculations a hybrid error estimator, which considers both fluid dynamic and radiative errors, will need to be developed. For pure radiation calculations presented in this paper, the local truncation error is estimated using gradients of the radiant intensity.

3.2 Grid Structure and Nomenclature

The grid structure may be characterized by a nested hierarchy of refined subgrids. The entire spatial domain is first covered by a set of disjoint grids of uniform refinement. A finer refinement level (defined by another set of grids) is then placed over the coarser level in locations where higher resolution is required. The finer set of grids is itself disjoint, but need not be contiguous, and its resolution is described by an integral refinement ratio with respect to the coarse grid. Fine grids may overlap more than one coarse grid and may be located adjacent to physical boundaries. Finer and finer refinement levels are recursively placed upon one another until the desired resolution is obtained. A example grid structure is shown in Figure 1. The nesting procedure is detailed by Berger and Colella (1989).

The computational domain on a given level is denoted by the union of a disjoint set of rectangular grids:

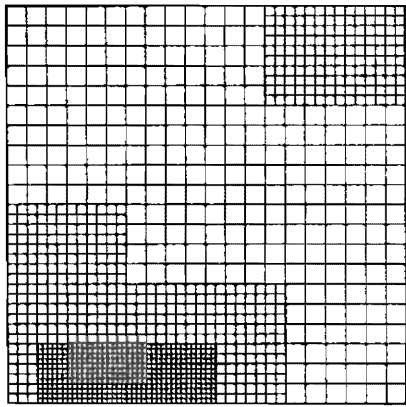
$$\Lambda^l = \bigcup_{i=1}^{N^l} \Lambda_i^l \quad (6)$$

where l and N^l are the level and number of grids comprising the level, respectively. Portions of this domain may be covered by grids of a finer refinement level ($l+1$). The area of overlap is defined by the projection of the finer level ($l+1$) to the coarser (l) and is denoted by $P(\Lambda^{l+1})$. The interior and exterior composite boundaries of the level are given by:

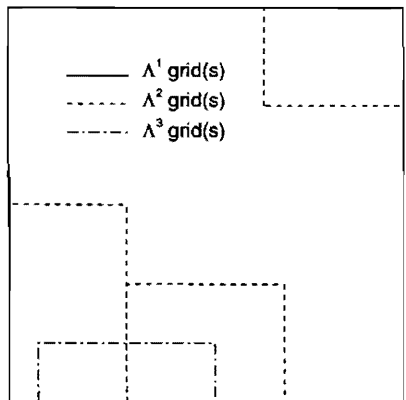
$$\partial\Lambda^{l,i} = \bigcup_{i=1}^{N_i} \left(\partial\Lambda_i^l \cap \partial\Lambda_j^l \right) \quad (7)$$

$$\partial\Lambda^{l,e} = \left(\bigcup_{i=1}^{N^l} \partial\Lambda_i^l \right) - \partial\Lambda^{l,i} \quad (8)$$

where $\partial\Lambda_i^l$ represents the boundary of Λ_i^l . The interface between two levels of differing refinement (levels l and $l+1$) is represented by the exterior boundary of the finer level ($l+1$). The projection of this interface to the coarser level is required for the communication between levels and is denoted by $P(\partial\Lambda^{l+1,e})$.



(a) Computational grid



(b) Outlines of rectangular grids

Figure 1. Sample mesh hierarchy (2 refinement levels).

3.3 Single Grid Radiation Integrator

The integration of the DO equations is based on standard finite volume techniques employed by Fiveland (1984, 1988), Fiveland and Jessee (1995a), and others. The radiation integrator is independent of the AMR shell, operating on single rectangular grids. When given a grid, suitable boundary conditions, and an ordinate direction by the AMR algorithm, the integrator solves an ordinate transport equation [Equation (3)] over the rectangular patch. The integrator only operates on a single ordinate direction rather than the entire set. The reason becomes clear when the composite grid algorithm is detailed.

The spatially-discrete ordinate equation is obtained by integrating Equation (3) over a typical control volume:

$$\frac{\mu_m}{\Delta x}(I_{m,i+1/2,j} - I_{m,i-1/2,j}) + \frac{\xi_m}{\Delta y}(I_{m,i,j+1/2} - I_{m,i,j-1/2}) = \kappa I_b - \beta I_{m,jj} + S_m \quad (9)$$

Similar equations may be written for all volumes within the single grid. Assuming given boundary, emission, and in-scattering conditions, the system of equations is closed by defining an interpolation scheme that relates the face intensities to the nodal values. Common approaches include the step, exponential, and diamond difference techniques. Because the exponential and diamond difference schemes are unbounded and often lead to oscillatory solutions, they are avoided in the present work, and the first-order step (upwind) scheme is exclusively applied. Although the step scheme is bounded, it has the disadvantage of being only first-order accurate. Since this paper is primarily concerned with algorithmic details and robustness of the methods, the use of the step scheme is appropriate. In practice, bounded, high resolution (HR) differencing schemes should be applied. Such schemes have recently been applied in a single-grid context by Fiveland and Jessee (1995a) and Jessee and Fiveland (1996). Future work will apply HR schemes to the current AMR algorithm.

For the step scheme, a given ordinate equation may be solved using a single sweep over the grid in which volumes are visited from upstream to downstream (Fiveland, 1984). The process is analogous to ordering the equations from upstream to downstream to provide an upper triangular matrix, and then back solving the system of equations. Multiple iterations are required to include the influence of in-scattering and wall reflections.

3.4 Multiple-level Algorithm

The purpose of the multiple-level algorithm is to obtain a solution to the discrete RTE over the composite grid structure. This should not be confused with multigrid algorithms whose purpose is to accelerate solutions, although multigrid techniques may be used in conjunction with the present multiple-level algorithm. The multiple-level problem may be expressed as:

$$L_m^l(I_m^l) = \kappa I_b^l + S_m^l \quad \text{on } \Lambda^l - P(\Lambda^{l+1}) \quad (10)$$

$$I_m^l = \langle I_m^{l+1} \rangle \quad \text{on } P(\partial\Lambda^{l+1}), \quad l < l_{\max} \quad (11)$$

for all m where $\langle \cdot \rangle$ denotes a spatial averaging operator. These governing equations state that the RTE must be satisfied on any *uncovered* portion of the composite grid, and the intensity field must

be continuous at interfaces between levels of differing refinement -- the flux leaving one portion of the computational domain must equal the flux entering the adjacent portion. This statement neglects the solution on a portion of any level that is *covered* by a level of finer refinement, namely in the region $P(\Lambda^{l+1})$.

The present multiple-level algorithm is based on the approach of Bell et al. (1994), and differs substantially from the standard single-level algorithm for the DO method (Fiveland, 1984, 1988). For a given ordinate direction, the standard solution algorithm sweeps the spatial grid from upstream to downstream. This approach may be extended to an embedded grid with the modifications that when a ray passes from a coarse to fine grid, the interface intensity is interpolated, and when a ray passes from a fine to coarse grid, the interface intensity is averaged. One spatial sweep provides the composite solution to the ordinate equation over the composite grid. More sweeps would be required to include the influence of explicitly-treated wall reflection and in-scattering terms. This approach has disadvantages from efficiency and programming standpoints. Because the interpolation and averaging operations are embedded in the sweep of the spatial grid, computation loops in solution process are extremely small or are broken by conditional blocks of code. This not only limits the degree of vectorization and parallelization, but also greatly increases the complexity of the coding.

The proposed multiple-level algorithm differs from the standard one in that levels in the grid hierarchy are operated on individually. For instance, in a two-level algorithm, the process begins by solving the RTE over the entire coarse level. Next the conditions at the coarse-fine interface are interpolated and applied to the boundary of the fine level, and the RTE is solved on this level. Fluxes leaving the fine level are then averaged and applied to the coarse grid to ensure conservation, and the coarse grid solution is again found, this time with the influence of the fine level. The transfer of information between levels is similar to the approach detailed by Bell et al. (1994) and Berger and Colella (1989). At coarse/fine interfaces, intensities are interpolated with a piecewise constant operator, while averaging is performed using an area-weighted operator. Iteration between the levels continues until the composite solution is converged. This domain decomposition approach has the disadvantage that iteration between the levels is required. Nevertheless, studies have shown that for cases with partially reflecting walls and/or scattering media, global convergence of the method is comparable with the single grid algorithm. The approach has the advantage that the sweeping, interpolation, and averaging operations are applied over large regions with uniformly spaced grids.

Formally, the multiple-level algorithm proceeds as follows:

- Compute emission and scattering sources on each level.
- Perform single space-angle sweep on coarsest level Λ^1 .
- Transfer (interpolate) solution to boundary $\partial\Lambda^{2,c}$.
 - Perform single space-angle sweep on level Λ^2 .
 - Transfer (interpolate) solution to boundary $\partial\Lambda^{3,c}$.
 - ⋮
 - Perform single space-angle sweep on level $\Lambda^{l_{\max},e}$.
 - Average fluxes at downstream boundaries for coarser level.
 - ⋮
 - Perform single space-angle sweep on level Λ^2 .
 - Average fluxes at downstream boundaries for coarser level.
- Return to beginning of cycle if not converged.

On the first sweep of the coarse level, the coarse/fine interface is

neglected since no information from the finer level is available at this time.

In general, the single space-angle sweep on a given level involves the solution on more than one rectangular grid. Special sequencing of the solution on the level is necessary to guarantee the efficient transfer of information across the domain. If the grids are not adjacent to one another, the boundary conditions are established by either the coarser level conditions or by the physical boundary conditions, and sequencing is immaterial. However, if the grids are adjacent, the upstream conditions for one grid are provided from the downstream conditions of another. This dependence necessitates that the solution over the grids proceeds in an ordered fashion; the upstream grids must be swept first. Because the upstream direction varies with ordinate direction, different orderings are required for different ordinate directions. The number of unique orderings is 2^n where n is the spatial dimension (e.g., $n=2$ for two-dimensional space). The orderings correspond to the principal directions (e.g., all possible permutations of $(\pm 1, \pm 1)$ for two-dimensions), and may be denoted by the sets C_j^i , $j=1, \dots, 2^n$. Each set C_j^i contains a list of ordered grids for the particular principal direction. In addition, each ordinate direction may be assigned one of these ordered sets -- a relationship denoted by the pointer j_m -- by inspecting the signs of the respective direction cosines. Whenever a new grid structure is generated, these grid orderings may be predetermined for each level. During the level space-angle sweep, the solution sequence first loops over ordinate directions and then over the ordered grids for the given direction:

```

For  $m \in \{1, \dots, M\}$  do
  For  $i \in C_{j_m}^i$  do
    • Obtain upstream boundary conditions from adjacent
      upstream grids on same level.
    • Solve ordinate equation  $m$  on grid  $i$ :
       $L_m^i(I_m^i) = \kappa I_b^i + S_m^i$  on  $\Lambda_i^i$ 
  Enddo
Enddo

```

3.5 Error Estimator

The local truncation error (LTE) is measured by the normalized gradient of the radiant intensity:

$$LTE_m = \Delta x \frac{|\nabla I_m|}{I_m} \quad (12)$$

where Δx denotes the characteristic cell size. To provide a single error estimator, an average LTE is defined:

$$\overline{LTE} = \frac{1}{M} \sum_{m=1}^M LTE_m \quad (13)$$

In the adaptive algorithm, the mesh is refined in portions of the domain where the following inequality is satisfied:

$$\overline{LTE} > \theta \quad (14)$$

where θ is a user specified error tolerance. This estimator should be fairly accurate for the first-order step scheme, but will be overly

conservative when high-order schemes are applied. For high-order differencing schemes, other estimators, such as one based on the finite volume analogue of the Zhu-Zienkiewicz estimator (Zienkiewicz and Zhu, 1987), will be more appropriate.

4.0 RESULTS

The radiation algorithm is investigated by considering two standard benchmark cases and a case to "simulate" a coupled transient analysis:

- 1) Black rectangular enclosure with a purely absorbing medium
- 2) Gray, rectangular enclosure with a purely scattering medium
- 3) Black enclosure with a moving emission source

The first two cases are extensively analyzed while the last case is presented to graphically illustrate the AMR process. For the benchmark cases, the evaluation is based on the following criteria:

- 1) Accuracy
- 2) Total computation time
- 3) Convergence characteristics

Results are compared to the exact solutions and predictions from other workers. Global energy balances are resolved to machine round-off for the converged solutions. Convergence is measured by the normalized difference in the incident energy from two successive space-angle sweeps:

$$|R|_{\infty} = \max\{R_i : i=1, \dots, N_{cell}\} < 10^{-6} \quad (15a)$$

where

$$R_i = \frac{|G_i^{n+1} - G_i^n|}{G_i^{n+1}} \quad (15b)$$

and superscripts n and i denote the iterate and cell index, respectively. The level-symmetric even S_4 ordinate set (Fiveland, 1991) was used for all cases unless otherwise indicated. A short description of the individual cases follows.

4.1 Black Rectangular Enclosure with an Absorbing Medium

The case consists of a two-dimensional, rectangular enclosure with cold walls and a purely absorbing medium maintained at an emissive power of unity (Fiveland, 1984; Fiveland and Jessee, 1995a). Absorption coefficients, κ , of 1 and 10 are individually be considered.

For the case of black walls, spatially exact solutions to the S_n equations are available (see Appendix A). This is not the "exact" solution to the RTE, but the spatially exact solution to the angular approximation. Therefore, it may be used to measure the error due solely to a given spatial discretization (i.e. the computational mesh and spatial differencing order). Measurement of angular discretization error, namely ray effects, is another topic and should be considered separately. To quantify the spatial discretization (SD) error, the following error definition is used:

$$E(x,y) = \frac{|G(x,y) - \overline{G}(x,y)|}{\overline{G}(x,y)} \times 100\% \quad (16)$$

where \overline{G} and G represent the spatially exact and approximate DO

solutions, respectively. In addition, the following norms are defined:

$$|E|_1 = \frac{\sum V_i E_i}{\sum V_i} \quad (17)$$

$$|E|_\infty = \max\{E_i : i=1, \dots, N_{cell}\} \quad (18)$$

The summations in Equation (17) extend over all cells in the computational domain.

Optical thicknesses of 1 and 10 were individually analyzed on uniform grids of 10x10, 20x20, 40x40, 80x80, and 160x160 and adaptive grids found with error tolerances (θ) of 0.2, 0.1, 0.05, and 0.025. The accuracy and timing results are shown in Table 1 for κ of 1. The table displays the two error norms, total CPU time, and the number of computational cells. For the adaptive analyses, the CPU time includes the time required for all refinement cycles, the number of cells corresponds to the mesh for the last refinement cycle, and the final number of refinement levels is shown in parenthesis. The number of cells is displayed to quantify the memory requirements. All adaptive cases employ a refinement ratio of 2.

As expected, SD error is reduced as the grid resolution is increased. The adaptive algorithm is effective in reducing both the maximum and average error norms; however, the adaptive analyses generally require more CPU time than the uniform analyses with comparable error. Such undesirable behavior is due to two factors: first, several cycles are required for the adaptive algorithm to built up the refined mesh hierarchy; and second, multiple iterations are required at each cycle to transfer information over the refinement levels. The increase due to the first factor will be non-existent during transient analyses because refinement is intertwined in the time-stepping procedure. The increase due to the second factor will be largely mitigated when either partially reflecting walls and/or scattering media are considered since the convergence on a given grid structure is generally governed by the explicitly treated reflection and scattering terms as will be shown later.

The ability of the adaptive algorithm to reduce memory

Table 1
Error and Timing Statistics for Case 1 ($\kappa = 1$).

grid	$ E _1$	$ E _\infty$	CPU time (s)	no. of cells
10x10	3.140	13.34	0.13	100
20x20	2.041	11.29	0.43	400
40x40	1.201	7.296	1.68	1600
80x80	0.6775	4.073	6.91	6400
160x160	0.3718	2.280	28.34	25600
$\theta=0.2$	1.891	5.154	38.49	2500 (4)*
$\theta=0.1$	1.009	2.894	58.52	5396 (4)
$\theta=0.05$	0.5813	2.024	102.61	11892 (4)
$\theta=0.025$	0.3213	1.0983	309.17	48244 (5)

* Value in parenthesis denotes final number of refinement levels.

Table 2
Convergence Characteristics for Case 1
(Iterations for convergence).

κ	$\epsilon=0.1$		$\epsilon=0.5$		$\epsilon=1.0$	
	SG	AMR	SG	AMR	SG	AMR
0.1	63	62	19	19	1	5
1	17	17	11	10	1	5
10	10	8	8	8	1	5

SG = Single Grid Algorithm; AMR = Adaptive Mesh Algorithm

requirements is shown in the last column of Table 1. The comparison of the uniform 160x160 and adaptive $\theta=0.05$ cases reveals that similar error norms are obtained with the adaptive algorithm using less than half the cells of the uniform grid. Howell and Bell (1996) observed similar trends with respect to CPU time and memory requirements for the adaptive solution of the incompressible Navier-Stokes equations. Figures 2 and 3 display the final grid structures and incident energy fields for optical thicknesses of 1 and 10, respectively. An error tolerance (θ) of 0.05 was used to generate the results. As seen in these figures, the grid adapts to the steep gradients in the solution. Four levels of refinement are shown.

Convergence characteristics are measured by comparing the number of iterations required for convergence from the adaptive algorithm to that of the single grid algorithm. A range of absorption coefficients and wall emissivities is considered. The single and multiple-level grids used in the study correspond to the 40x40 uniform mesh and the final adaptive meshes for $\theta=0.05$, respectively. The number of refinement levels for the adaptive algorithm was constrained to four (although some conditions do not required four levels), and the number of iterations corresponds to the last refinement cycle. Table 2 displays the results. For the case of black walls, convergence is degraded slightly for by the multiple-level algorithm; however, for the gray cases, convergence is comparable. When the walls are gray, convergence is governed by the explicit treatment of the reflected boundary rays rather than by any communication delay caused by the multiple-level algorithm. For some conditions, the convergence of the multiple-level algorithm is actually better than the single grid algorithm.

4.2 Rectangular Enclosure with a purely Scattering Medium

The second case consists of a square enclosure with black walls and an isotopically scattering medium. The lower wall has an emissive power of unity, and the other walls have zero emissive power. All walls of the enclosure have an emissivity of 1. The case has been analyzed by a number of workers (Fiveland, 1984; Fiveland and Jessee, 1995a; Ratzel and Howell, 1982) and serves as a good benchmark for scattering applications.

Because exact solutions are not available to this problem, the accuracy may not be quantified exactly. To compensate, the SD error is measured by comparing DO results to those from a 320x320 uniform grid and the second-order CLAM scheme (Jessee and Fiveland, 1996). This solution is taken as the benchmark to which all other solutions are compared using the error norms of Equations (17) and (18).

The case was analyzed on both uniform and adaptive grids. Error

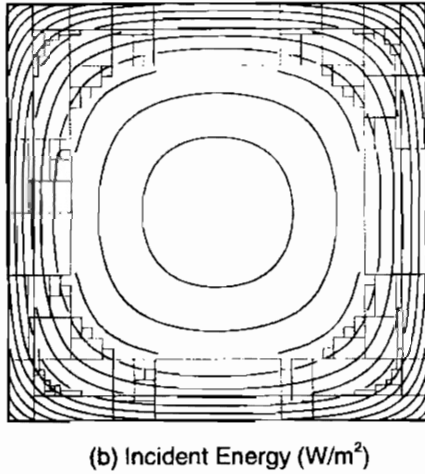
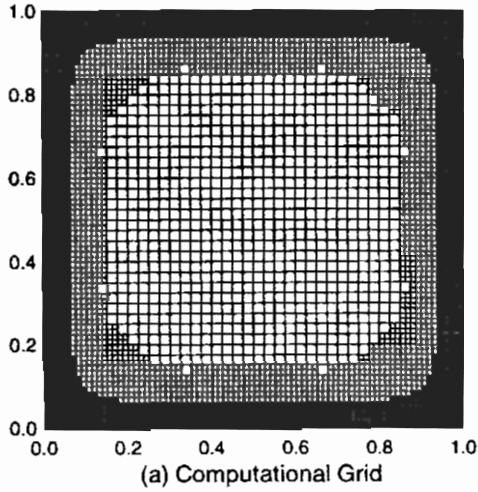


Figure 2. Refined grid and solution for Case 1 ($\kappa=1, \theta=0.05$).

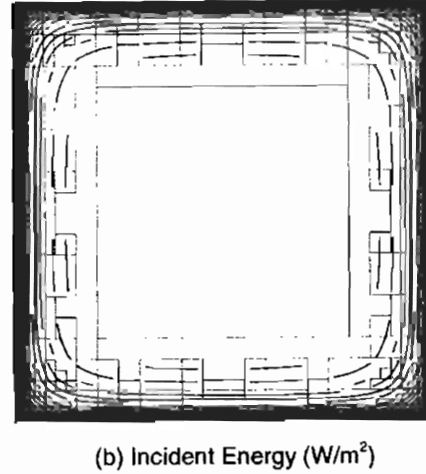
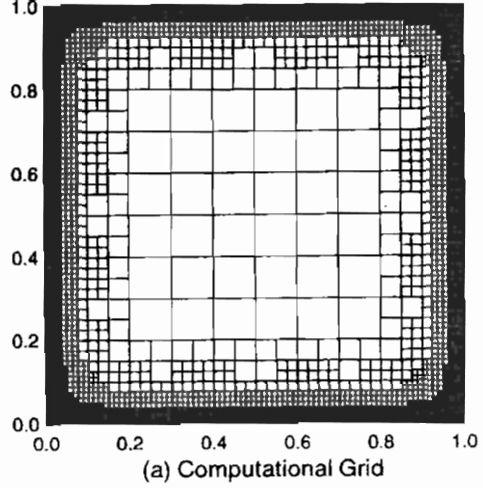


Figure 3. Refined grid and solution for Case 1 ($\kappa=10, \theta=0.05$).

and timing results are shown in Table 3. As displayed in the table, the adaptive algorithm generally requires more CPU time for a given level of error compared to the single grid algorithm. As stated previously, the increase in CPU time is largely due to the additional solutions that are needed in the refinement process, and will be mitigated in transient calculations. Figure 4 displays the final adapted grid structure and the resulting incident energy field. High gradients are visible near the lower wall which has the driving emissive power. Outlines of the grid structure are overlaid on the incident energy contour.

Convergence characteristics for the single and multiple-level algorithms are shown in Table 4. A range of scattering coefficients and wall emissivities is considered. The single and multiple-level grids used in the study correspond the 40x40 uniform mesh and the final adaptive meshes for $\theta=0.05$, respectively. The number of refinement levels for the adaptive algorithm was constrained to four, and the number of iterations corresponds to the last refinement cycle. The table indicates that the convergence is generally not affected by multiple-level algorithm. The explicitly treated in-scattering and

**Table 3
Error and Timing Statistics for Case 2 ($\sigma = 5$).**

grid	$ E _1$	$ E _2$	CPU time (s)	no. of cells
10x10	11.35	44.71	5.94	100
20x20	6.243	28.54	22.54	400
40x40	3.313	16.29	89.79	1600
80x80	1.756	10.32	364.28	6400
160x160	0.9376	6.800	1529.28	25600
$\theta=0.1$	9.087	38.67	32.28	172 (2)*
$\theta=0.05$	5.724	26.42	89.57	664 (2)
$\theta=0.025$	3.344	15.13	438.50	2780 (3)
$\theta=0.01$	1.459	13.79	1745.33	14860 (4)

* Value in parenthesis denotes final number of refinement levels.

Table 4
Convergence Characteristics for Case 2
(Iterations for convergence).

σ	$\epsilon=0.5$		$\epsilon=0.75$		$\epsilon=1.0$	
	SG	AMR	SG	AMR	SG	AMR
0.1	20	20	12	12	7	7
1	43	38	27	22	19	17
10	327	257	258	199	223	169

SG = Single Grid Algorithm; AMR = Adaptive Mesh Algorithm

reflection terms dominate the convergence. For some conditions, the multiple-level algorithm requires fewer iterations. Although they were not applied here, mesh rebalance techniques (Fiveland and Jessee, 1995b) may be used to accelerate convergence for problems

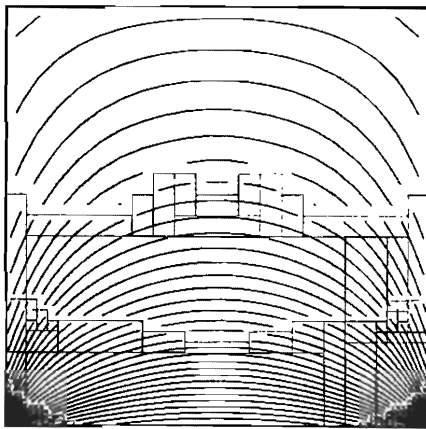
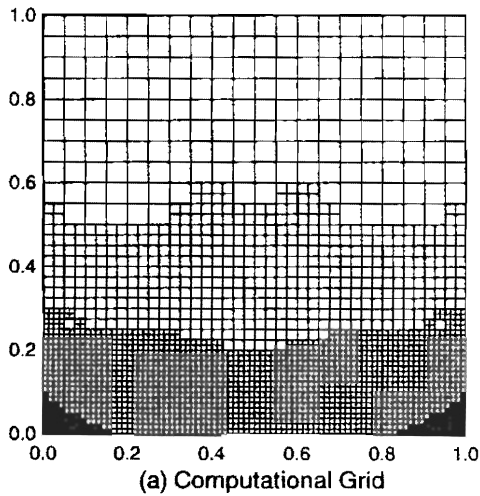


Figure 4. Refined grid and solution for Case 2
 $(\sigma=5, \theta=0.025)$.

with significant scattering. Such acceleration techniques will likely prove effective for the multiple-level grid structure and should be investigated in future work.

4.3 Black Enclosure with Time-Varying Emission

Radiative transfer is considered in a rectangular enclosure with a moving area source. The case was selected to conceptually simulate a moving flame front in a combustion analysis, and to illustrate the adaptation process. The conditions are displayed in Figure 5. A circular area of radius 0.1 and emissive power of 5 moves in a path of radius 1/3 and origin located in the center of the enclosure. The emissive power of the surrounding media and walls is unity, the absorption coefficient (κ) of the entire domain is 10, and the walls are black. The "spot" moves at a frequency of 1 rotation per second.

Figure 6 displays the adapted grids and predicted incident energy fields at four times in the rotation cycle -- $t=0, 0.125, 0.25,$ and $0.375s$. The case was analyzed with an error tolerance (θ) of 0.05, and the number of refinement levels was constrained to three. At each timestep, four adaptation cycles were allowed. As shown in Figure 6, the algorithm adapts the grid to the area of high emission and accurately captures the steep gradients in the solution. The incident energy is high in the vicinity of the area source and decays as rays penetrate the surrounding media. Rotational symmetry of 90 degrees may be seen by comparing the results which differ by a 0.25s time interval (e.g., results at $t=0$ and $t=0.25s$).

5.0 SUMMARY

An adaptive mesh refinement algorithm has been formulated and implemented for the discrete ordinates method. The resulting algorithm has exhibited convergence characteristics comparable to those of the single grid algorithm. In addition, the algorithm has illustrated the ability to adapt to areas of high local truncation error based on a simple error estimator. However, for the two basic benchmark cases considered, the AMR algorithm did not show any efficiency gain over the single grid algorithm, although memory requirements were reduced. This anomaly is due to the nature of the benchmark problems - large areas of uniform emissive power - and to the added computation of the refinement cycles. The last case

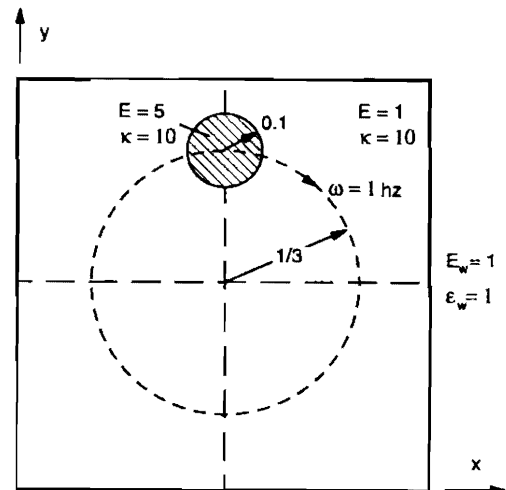
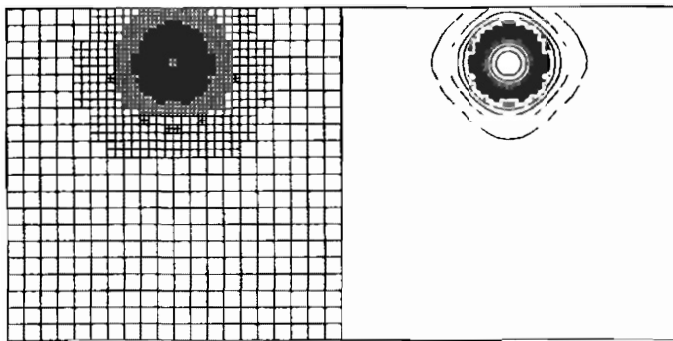
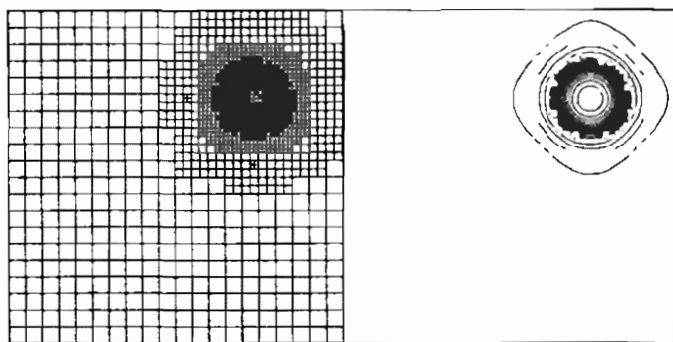


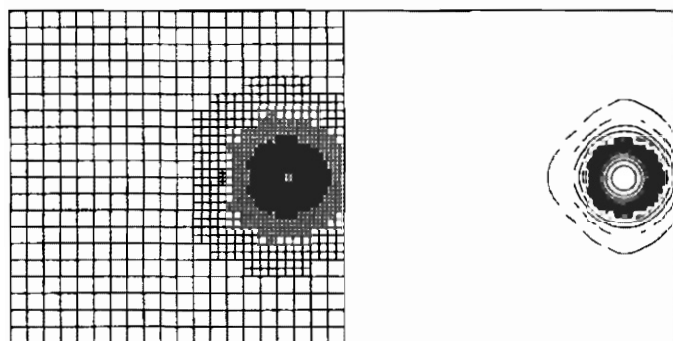
Figure 5. Geometry and conditions for Case 3.



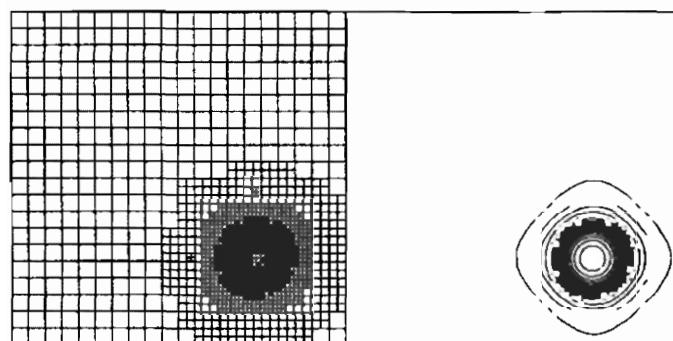
(a) $t = 0.0$ s



(b) $t = 0.125$ s



(c) $t = 0.25$ s



(d) $t = 0.375$ s

Figure 6. Refined grid (left) and predicted incident energy (right) for Case 3 ($\theta=0.05$).

illustrated adaptation to a moving front and provides a prelude to integrating the DO algorithm into a combustion dynamics code. The efficiency gains of the AMR algorithm will not be fully realized until coupled, three-dimensional, transient calculations are performed. This application is a topic of future work.

ACKNOWLEDGEMENTS

This work was partially funded by the U.S. Department of Energy's Mathematical, Information, and Computer Science Division (Contract No. W-7405-ENG-48) through a subcontract from Lawrence Livermore National Laboratory (Subcontract No. B307848).

REFERENCES

- Bell, J., Berger, M., Saltzman, J. and Welcome, M., 1994, "Three-Dimensional Adaptive Mesh Refinement for Hyperbolic Conservation Laws," *SIAM J. Sci. Comput.*, Vol. 15, No. 1, pp. 127-138.
- Berger, M.J., and Colella, P., 1989, "Local Adaptive Mesh Refinement for Shock Hydrodynamics," *J. Comput. Phys.*, Vol. 83, pp. 64-84.
- Fiveland, W.A., 1984, "Discrete-Ordinates Solutions of the Radiative Transport Equation for Rectangular Enclosures," *Transactions of ASME, Journal of Heat Transfer*, Vol. 106, pp. 699-706.
- Fiveland, W.A., 1988, "Three-Dimensional Radiative Heat Transfer Solutions by the Discrete-Ordinates Method," *Journal of Thermophysics and Heat Transfer*, Vol. 2, No. 4, pp. 309-316.
- Fiveland, W.A., 1991, "The Selection of Discrete Ordinate Quadrature Sets for Anisotropic Scattering," *ASME HTD-Vol. 72*, pp. 89-96.
- Fiveland, W.A., and Jamaluddin, A.S., 1991, "Three-Dimensional Spectral Radiative Heat Transfer Solutions by the Discrete Ordinates Method," *Journal of Thermophysics and Heat Transfer*, Vol. 5, No. 3, p. 335-339.
- Fiveland, W.A. and Jessee, J.P., 1995a, "A Comparison of Discrete Ordinates Formulations for Radiative Heat Transfer in Multidimensional Geometries," *Journal of Thermophysics and Heat Transfer*, Vol. 9, No. 1, pp. 47-54.
- Fiveland, W.A. and Jessee, J.P., 1995b, "Acceleration Schemes for the Discrete Ordinates Method," *ASME HTD-Vol. 315, Proceedings of the 30th National Heat Transfer Conference*, Volume 13.
- Fuchs, L., 1986, "A Local Mesh Refinement Technique for Incompressible Flows," *Comput. Fluids*, 14, pp. 69-81.
- Howell, L.H. and Bell, J.B., 1996, "An Adaptive Mesh Refinement Projection Method for Viscous Incompressible Flow," *SIAM J. Sci. Comput.*, to appear.
- Jessee, J.P. and Fiveland, W.A., 1996, "Bounded, High Resolution Differencing Schemes Applied to the Discrete Ordinates Method," *1996 National Heat Transfer Conference*, Houston, TX, August 3-6.
- Kallinderis, Y., 1992, "A Finite Volume Navier-Stokes Algorithm for Adaptive Grids," *Int. J. Numerical Methods in Fluids*, 15, pp. 193-217.
- Lewis, E.E., and Miller, W.F., 1984, *Computational Methods of Neutron Transport*, John Wiley & Sons.
- Modest, M.F., 1993, *Radiative Heat Transfer*, McGraw-Hill.
- Ratzel, A.C. and Howell, J., 1982, "Two Dimensional Radiation in Absorbing-Emitting-Scattering media using the P-N approximation," *ASME paper No. 82-HT-19*.
- Zienkiewicz, O.C. and Zhu, J.Z., 1987, "A simple estimator and adaptive procedure for practical Engineering Analysis," *Int. J. Num.*

APPENDIX A - EXACT SOLUTION TO CASE 1.

The exact solution to the discrete ordinates equation is:

$$I_m(x,y) = (I^o - I_b) e^{-xs} + I_b \quad (A1)$$

where

$$s = \min \left(\frac{x-x^o}{\mu_m}, \frac{y-y^o}{\xi_m} \right) \quad (A2)$$

and

$$x^o = \begin{cases} 0 & \mu_m > 0 \\ X_L & \mu_m < 0 \end{cases} \quad y^o = \begin{cases} 0 & \xi_m > 0 \\ Y_L & \xi_m < 0 \end{cases} \quad (A3)$$

The incident energy from the exact spatial solution of the DO equations may be found by forming the angular quadrature of the above intensity expression:

$$G(x,y) = \sum_{m=1}^M w_m I_m(x,y) \quad (A4)$$